PAPER

lco⊕®≡

Current density at failure of twinned silver nanowires

To cite this article: Mohammad Waliullah and Rodrigo A Bernal 2022 Nanotechnology 33 305706

Manuscript version: Accepted Manuscript

Accepted Manuscript is "the version of the article accepted for publication including all changes made as a result of the peer review process, and which may also include the addition to the article by IOP Publishing of a header, an article ID, a cover sheet and/or an 'Accepted Manuscript' watermark, but excluding any other editing, typesetting or other changes made by IOP Publishing and/or its licensors"

This Accepted Manuscript is@.

During the embargo period (the 12 month period from the publication of the Version of Record of this article), the Accepted Manuscript is fully protected by copyright and cannot be reused or reposted elsewhere.

As the Version of Record of this article is going to be / has been published on a subscription basis, this Accepted Manuscript will be available for reuse under a CC BY-NC-ND 3.0 licence after the 12 month embargo period.

After the embargo period, everyone is permitted to use copy and redistribute this article for non-commercial purposes only, provided that they adhere to all the terms of the licence https://creativecommons.org/licences/by-nc-nd/3.0

Although reasonable endeavours have been taken to obtain all necessary permissions from third parties to include their copyrighted content within this article, their full citation and copyright line may not be present in this Accepted Manuscript version. Before using any content from this article, please refer to the Version of Record on IOPscience once published for full citation and copyright details, as permissions may be required. All third party content is fully copyright protected, unless specifically stated otherwise in the figure caption in the Version of Record.

View the article online for updates and enhancements.

Current density at failure of twinned silver nanowires

Mohammad Waliullah¹, Rodrigo Bernal¹

¹Department of Mechanical Engineering, The University of Texas at Dallas, Richardson, TX 75080, USA

Email: bernal@utdallas.edu

ABSTRACT

Silver nanowires have a wide range of potential applications in stretchable and transparent electronics due to their excellent electrical, mechanical, and optical properties. For a successful application in electronic devices, evaluating the electrical reliability of these nanowires is required. We have studied experimentally the behavior of current density at failure for penta-twinned silver nanowires with diameters between 53 nm and 173 nm, for 93 samples. The current densities at failure are widely scattered, have an average of 9.7 x 10⁷ Acm⁻², and a standard deviation of 2.96 x 10⁷ Acm⁻². Heat- transfer modelling is employed to explain the results, and Weibull statistics are used to quantify failure probabilities, thus offering guidelines for future designs based on these nanowires. The scatter observed in the measurements is attributed to surface-roughness variations among samples, which lead to local hot-spots of high current density. These results quantify the Joule-heating electrical reliability of silver nanowires and highlight the importance of heat transfer in increasing it.

Keywords: nanoscale heat transfer, electrical reliability, stretchable electronics, wearable electronics, transparent electronics, burnout current density

1. INTRODUCTION

Recently, high aspect ratio nanostructures like nanowires [1], carbon nanotubes [2] and nanopillars [3] have attracted interest, due to their outstanding electrical, mechanical and optical properties, which make them suitable for a wide range of applications, for example in the fields of nanoelectronics [1], bio-sensing, and nanomedicine [3]. Among various types of high aspect ratio nanostructures, metallic nanowires are envisioned as components in, among others, flexible electronics, photovoltaics, organic LEDs, transparent heaters, and electromagnetic shielding [1].

In the area of transparent and stretchable/flexible electronics, 99.1% transmittance and 130 Ω sq⁻¹ sheet resistance was achieved when a silver nanowire network was deposited on a transparent substrate [4]. Thus, metallic nanowire networks, particularly made of silver, can rival the optoelectronic performance of ITO (95% transmittance and 50 Ω sq⁻¹), a material currently used widely in transparent electronics, thin-film solar cells, and organic LEDs. ITO is particularly costly and thus metallic nanowires can be used for next-generation transparent electronics [5] due to their superior optoelectronic performance as well as enabling cheaper solution-coating methods. In addition, these nanowires have high mechanical strength [6], high aspect ratio, and recoverable plasticity [7–9]. These properties enable the nanowires to maintain conductivity even under a high strain [10] when deposited on a flexible substrate. Thus, metallic nanowire networks are envisioned as the building blocks for future flexible and wearable electronics [1].

However, achieving consistent reliability is still a challenge. Detrimental, irreversible, electrical-resistance changes of the network are usually observed over time, due to failure of the individual nanowire constituents when current density (current per cross-sectional

area) is high [11]. Metallic nanowires under electrical stresses, primarily fail due to two reasons: 1) Joule heating and 2) electromigration [12]. Joule heating is the conversion of a portion of electrical energy into thermal energy and heating up of the wire as a result, which can lead to melting if current densities are high. On the other hand, electromigration is caused by momentum exchange between the electrons and the atoms during a flow of electric current. When there is a high current density, usually in the order of 10⁵ - 10⁶ A/cm², this momentum exchange causes the atoms to be displaced from their equilibrium position towards the direction of current flow [13]. When more and more atoms start diffusing in that direction, they leave behind vacancies which merge to form larger voids. As a result of this void formation, cross sectional area reduces and hence resistance of the electrical conductor starts to increase. Also, due to absence of matter in the voids, the voids try to collapse upon themselves creating a tensile stress acting upon the surrounding atoms. As a reaction, the atoms exert a tensile stress upon the voids. Eventually, because of this tensile stress, the electrical conductor is torn apart.

There are several reports which studied the electrical failure of gold [14,15], copper [16] and bismuth nanowires [17] and explored the above-mentioned reasons behind the failure. The joints between nanowires in conductive networks and their reliability have also been studied [18]. These reports also studied the diameter effect on the current densities at failure. They have found out that the current densities at failure generally increase with a decrease in the diameter of the nanowires due to increasing surface area to volume ratio.

However, given that they provide a solution-coatable alternative to ITO, their wide commercial availability, and their wide use in applications, reliability characterization of silver nanowires is also important. In particular, so-called penta-twinned silver nanowires, fabricated with the polyol method [19] have been extensively used in demonstrations of transparent, flexible and stretchable electronics [5,20], such as heaters [1] and wearable electrodes [21]. They have a pentagonal structure, which arises from the merging of 5 single crystals at twin boundaries [22]. Nevertheless, quantification of their electrical reliability over a broad range of diameters and large number of samples is still lacking, even though their electrical resistivity has been characterized carefully [22]. This information is critical for the design of reliable electronics based on silver nanowire networks if they are to display consistent behavior.

In our work, we studied current density at failure for penta-twinned silver nanowires between 53 and 173 nm diameter. A total of 93 individual nanowires were studied to extract the data. Our work thus provides a broad range of data on electrical reliability of silver nanowires for designers of flexible and wearable electronics.

2. EXPERIMENTAL METHODS

Each nanowire was connected to two gold pads on a silicon chip. The sample preparation can be divided into several phases which are described below.

2.1. Photolithography

Several silicon wafers with 300 nm thermally grown oxide were prepared by photolithography using a pre-designed mask with several contacting pads. A positive photoresist (S1813, Microchem Corp., Woburn, MA) was used for the process. MF-319 (Microchem Corp., Woburn, MA) was used as the developer. 120 nm of chrome-gold was e-beam evaporated after developing the pattern. Lift off with sonication was performed to get the final pattern with gold contact pads.

2.2. Nanowire deposition and mapping.

The microstructure and surface defects of the nanowires were investigated using a transmission electron microscope (TEM). Figure 1a shows the diffraction pattern obtained from one of the nanowires. Due to the penta-twinned structure, face-centered rectangular <112> and square <100> zone axes are superimposed with each other in the diffraction pattern, which is shown in figure 1b. Figure 1c shows that the central region has Moiré fringe patterns due to superimposition of single-crystal domains [23]. The insets show how the electron beam gets transmitted through the nanowires.

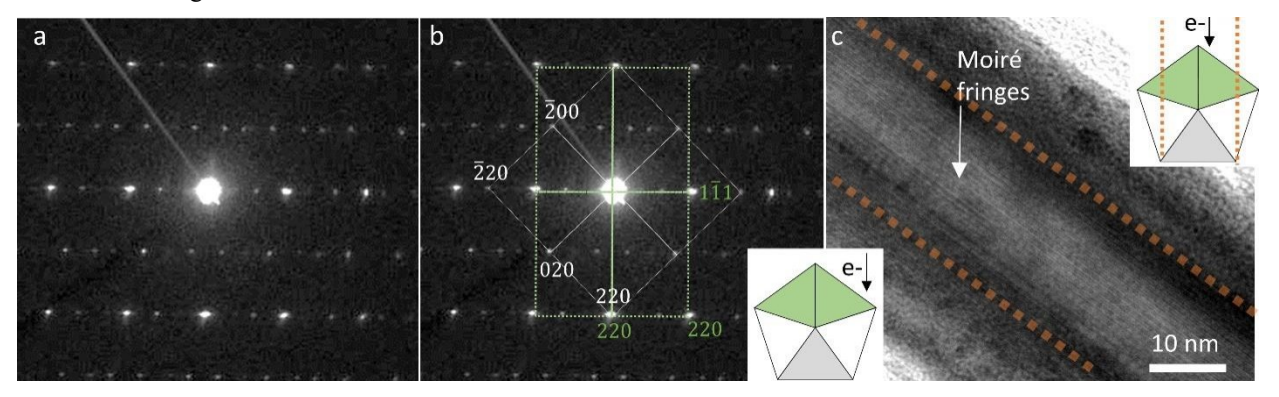


Figure 1: Microstructure characterization of silver nanowires showing a. Diffraction pattern. b. Superimposition of <112> (green rectangles) and <100> (white squares) zone axis patterns of an FCC structure on the diffraction pattern. Diffraction spots in the <112> and <100> zones are denoted with the same colors. c. TEM image of a silver nanowire showing fringe patterns due to superimposition of domains along different zone axes. The inset image shows the superimposed zone axis. The dashed lines represent the area of overlap in the direction of the electron beam, where the fringes appear.

The diluted nanowire solution (Sigma Aldrich, St. Louis, MO) was dispensed on a cut-to-size sample with electrodes prepared as mentioned above. Deposition was conducted with a pipette, followed by immediate N_2 drying to obtain a sparse coverage of individual nanowires without overlaps. Two different batches of nanowires from the same source were used. The nominal diameters are 115 nm (solvent IPA) and 70 nm (solvent ethanol), but each batch had a distribution of sizes between ~50 nm to 170 nm. The nanowires were characterized by TEM, and their penta-twinned structure was verified (see Supp. Mat.) The length between the electrodes was designed to be 4 μ m and determines the tested nanowire length for all experiments. The original solution (5 mg/mL) was diluted 250 times. After deposition, single nanowires in multiple locations were chosen for connections and their coordinates were saved. Using those coordinates, an e-beam mask was designed to connect the nanowires to the photolithography-defined contact pads.

2.3. E-beam lithography (EBL)

Raith 150two EBL system was used as the tool. A bilayer positive e-beam resist was spin coated on the substrate to obtain a good undercut for gentle liftoff. 495 PMMA A4 (Microchem Corp., Woburn, MA) was used as the bottom layer and 950 PMMA A2 (Microchem Corp., Woburn, MA) was used as the top layer. 10 kV and 30 μ m aperture were used for the e-beam exposure and a dose of 375 μ C/cm² was chosen so that the whole depth of the resist was cross-linked by the e-beam. This enabled us to obtain the designed width of the patterns and an optimal size of the resist undercut. MIBK:IPA 1:3 (SUMMUS/VWR, Sugar Land, TX) was used as the developer for the resist.

2.4. Metal deposition and lift off

AJA Orion sputtering tool was used for the metal deposition on the e-beam created pattern. About 100 nm of silver was deposited. EBR PG (Microchem Corp., Woburn, MA) was used for the lift off.

2.5. Electrical measurement

After the device was fabricated, electrical measurement was performed by connecting micromanipulator probes to the gold pads. The probes were then connected to a Keithley 2450 Source/Measuring Unit (SMU), which has a resolution of 500 nA and 5 μ V. Using the SMU, current was applied in a linearly increasing fashion with a 20 μ A increment until the nanowire under test failed. Each step lasted approximately 0.7 s. A video recording of the failure was obtained using an optical microscope at a magnification of 50X. The data was saved as csv files in a USB device and later transferred to a computer for analysis.

3. RESULTS AND DISCUSSION

3.1. Behavior of current density at failure as a function of diameter

We obtained close to a hundred (93) experimental data points to show the relationship between current density at failure and diameter of the nanowires. Individual silver nanowires of different sizes were connected to an external circuit using photolithography and e-beam lithography techniques (see EXPERIMENTAL METHODS – Figure 2a). The diameters of these nanowires ranged from 53 to 173 nm. Diameter measurement was performed with high accuracy using high magnification scanning electron microscopy (SEM) images. The methodology for measuring diameters is discussed in the supplementary material. The distance between electrodes is the same in all experiments (~4um)

We recorded in-situ optical microscope videos of each of the failures. For all the data reported, we ensured the video shows that failure initiates in the nanowires, in-between the two electrodes. (See associated contents for a representative video of failure, and snapshots in Figure 2b-e). Note that electromigration always occurs at the negative electrode [13], because material depletion occurs there, as a result of momentum transfer from electrons traveling from the negative to the positive electrode. Our observation that failure initiates between the electrodes are an element to support that the failures reported are dominated by Joule heating, because the temperature of the nanowire is highest at the mid-point of the nanowire (see modeling section). Figure 2a and f show SEM images before and after such a failure respectively. Interestingly, in Figure 2d, a thinning of the nanowire in between the electrodes is observed just one frame before failure (Figure 1e). Some particulate material in the burnt portion remains (Figure 2f).

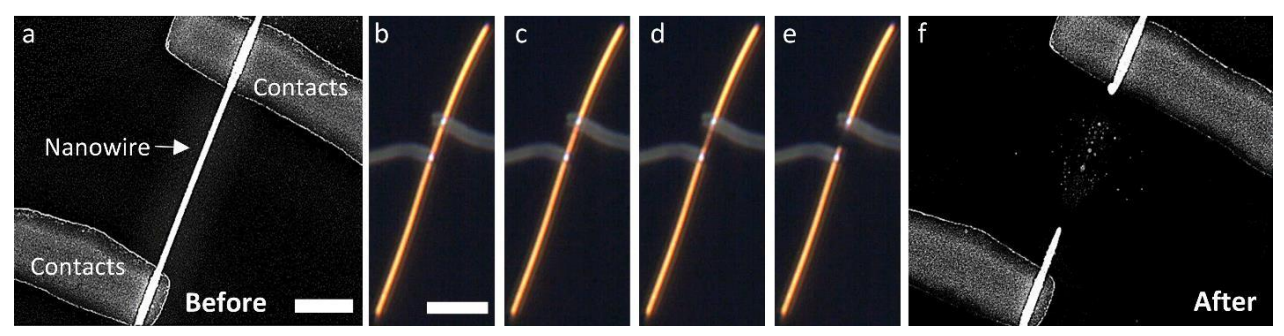


Figure 2: (a) SEM image of a nanowire at the beginning of electrical test (scale bar: $1\mu m$). (b) – (e) optical microscope images extracted from an in-situ video (see Supp. Mat.) of the same nanowire at different stages of the electrical test up to failure (scale bar: $10\mu m$). (f) SEM image of the nanowire after failure.

Figure 3a shows a plot of current density at failure vs. diameter for 93 data points. The current density at failure data was analyzed with Weibull statistics, to quantify the failure probabilities that our data provides. Heat transfer modelling will also be used to explain the results in subsequent sections. Note that the Weibull distribution is commonly used in electrical reliability measurements, such as Joule-heating failure of solder joints [24], dielectric breakdown [25], and electromigration [26]. In our case, we use the model [27,28]:

$$P_f = 1 - \exp\left(-\left(\frac{j - j_{th}}{j_0}\right)^m\right) \tag{1}$$

Here P_f is the probability of failure, j is the current density at failure measurement, j_{th} is a current density threshold below which no failure occurs, j_0 is a characteristic current density that signals the current density at which 63% probability of failure occurs.

Finally, m is the Weibull modulus, which indicates a measure of spread (larger exponent means less spread).

Our data was fitted to the above model using the maximum likelihood estimation method [27,28]. The results (Figure 3b) show a good fit to Weibull statistics. The fitted parameters are $j_{th} = 0$, indicating that failure of a nanowire at very low current densities cannot be discarded. $j_0 = 1.08 \times 10^8 \text{ A/cm}^2$, and m = 3.78. These parameters quantify probabilities of failure, and thus should help future device designs using silver nanowires. They also provide a comparison point for the effect of device-processing parameters in reliability. Beneficial processing steps should aim to increase all parameters, i.e., a maximum limit of operation for 100% nanowire survival j_{th} , a higher characteristic current density j_0 , and a reduction in behavior variability by increasing m.

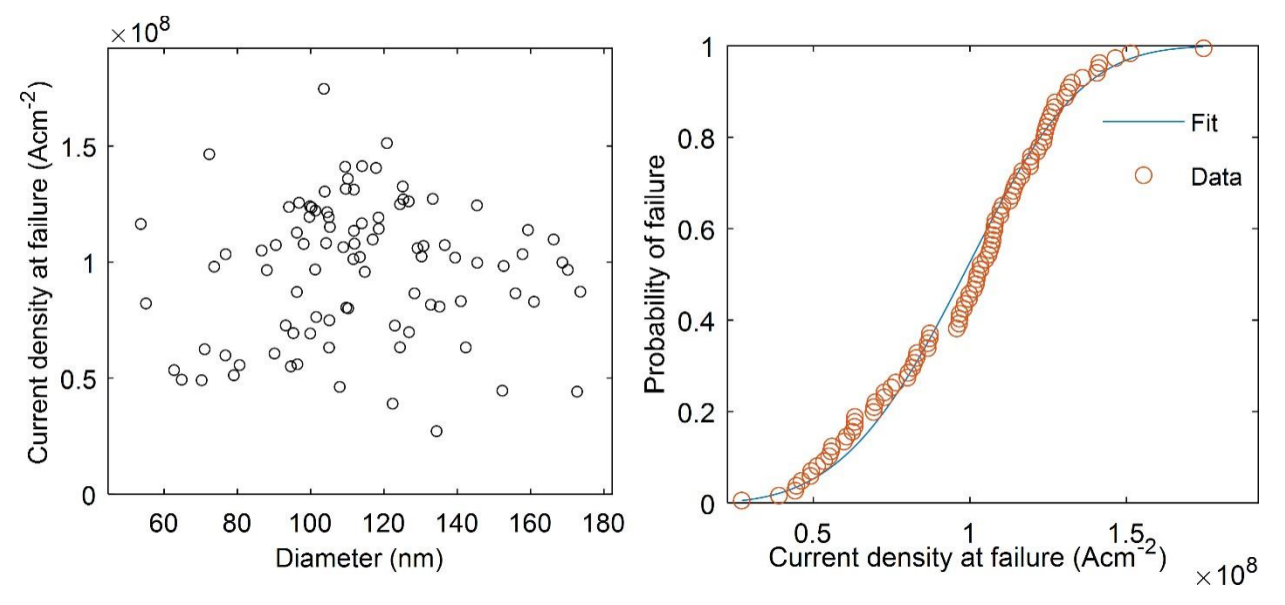


Figure 3: Plots of current density at failure, a. with respect to diameter. b. with respect to the probability of failure.

Note that we have bundled all results in one Weibull curve, because the size ranges explored in our research are limited. Recent results have shown that obtaining discernible differences in Weibull distributions requires testing a size span of 2-3 decades [29]. Our size variable is surface area, as the defects controlling failure arise from the surface (see discussion). However, given that we kept the gap between electrodes constant, the surface area varies less than one decade from 0.83 µm² to 2.72 µm². As a result, the above distribution can be considered as representative of the failures for nanowires typically used in nanowire networks, given that the diameters are similar and the gaps between nanowire joints are typically in the few-µm regime. However, the above distribution is insufficient to assess any statistical variations in current density to failure for more drastic changes in size. It is also insufficient to extract a controlling flaw size, as it is typically done in Weibull analyses of mechanical testing [30].

3.2. Theoretical modelling of diameter-dependent current density at failure

From the videos taken during the experiment, we hypothesized that the primary mode of failure in our experiment was Joule heating. The magnitudes of current density at failure obtained in Joule heating modelling (see below) suggest this is indeed the case.

The analysis assumes the nanowires survived (i.e. not melted) until they could effectively dissipate the heat generated due to the electricity. The heat can be dissipated into two sinks: 1) the electrical contacts and 2) the substrate [31,32], and the current densities to failure are controlled by the heat transfer to them. The electrical contacts were all fabricated in the same size and shape for all experiments. However, based on the size and shape of the nanowires, the heat transfer to the substrate may vary.

We frame the discussion based on three mathematical models, two of them aimed at bounding the extremes of behavior, and a third to model the real experimental conditions: Model 1 (Figure 4a) assumes that heat transfer only occurs through the contacts, and therefore models the extreme of poor substrate contact. Model 2 (Figure 4b) assumes heat transfer to the contacts plus a surrounding infinite medium at a fixed temperature at the ends of the wire, which then models maximum heat transfer to the substrate and contacts.

Model 3 (Figure 4c) conforms better with the nominal experimental conditions and assumes that only a portion of the nanowire has contact with the substrate.

a. Model 1 Electrode Electrode $T = T_{room}$ $= T_{room}$ Nanowire ρ, κ_{NW} Electrode b. Model 2 substrate Heat transfer ρ, κ_{NW} Substrate K_S c. Model 3 Substrate

Figure 4: Schematics of heat transfer models. a. Model 1 deals with electrode heat transfer. b. Model 2 models maximum heat transfer to electrodes and substrate. c. Model 3 depicts a nanowire with pentagonal cross-section having partial contact with the substrate, closely resembling the experimental conditions.

 $T = T_{room}$

3.2.1. Model 1: perfect electrode heat transfer and zero heat transfer to the substrate

In this model [31], shown in figure 3(a), the electrical contacts are assumed to be maintained at absolute temperature $T = T_{room}$, where T_{room} denotes room temperature. This model is based on the heat equation in cylindrical coordinates:

$$\frac{\partial^2 \Delta T(r,z)}{\partial r^2} + \frac{1}{r} \frac{\partial \Delta T(r,z)}{\partial r} + \frac{\partial^2 \Delta T(r,z)}{\partial z^2} = -p$$

where,

$$\Delta T = T - T_{room}$$

$$p = \frac{j^2 \rho}{\kappa_{NW}}$$
 4

Here, T, j, ρ and κ_{NW} denote temperature, current density, electrical resistivity, and thermal conductivity of the nanowire

respectively. At the interface of the nanowire and the substrate, the heat flux must be continuous. But if there is no heat transfer to the substrate and the heat is transferred to the electrical contacts only, then the heat flux at this interface must be zero. Thus, we can write the boundary condition:

$$\kappa_{NW} \frac{\partial \Delta T(r,z)}{\partial r} \Big|_{r=\frac{d}{2}} = 0$$

Since there is no heat transfer to the r direction, temperature will vary in only z direction. Applying the above-mentioned boundary condition, the solution to equation 2 at z = 0, where the temperature is maximum, can be expressed as:

$$\Delta T|_{z=0} = \frac{j^2 \rho L^2}{8\kappa_{NW}} \tag{6}$$

If we assume that the nanowire fails when it reaches its melting point temperature (500 °C [33]- See Supplementary Material) in the middle, we can substitute $\Delta T|_{z=0} = T_{melt} - T_{room}$ and establish an equation for the current density at failure, j_{fail} when there is heat transfer only to the electrical contacts:

$$j_{fail} = \sqrt{\frac{8}{L^2}} \left[\frac{(T_{melt} - T_{room}) \kappa_{NW}}{\rho} \right]$$
 7

For a constant L, this will be a constant line with no diameter dependence. However, it will depend on the value of ρ and κ_{NW} . These two properties vary with temperature and might be different for nanowires [33,34]. We considered the temperature ranges modeled, and the reported values of the properties for bulk and nanowires from several sources, including temperature variations where available, to establish absolute upper and lower bounds for these properties. The choices are explained and tabulated in detail in the supplementary material. Note that for this and all subsequent models, an upper bound for the current density at failure will be obtained with the best electrical conduction (lower bound for ρ) and heat conduction (higher bound for κ_{NW}). Similarly, the lower bound will be obtained with the worse electrical conduction (higher bound for ρ) and heat conduction (lower bound for κ_{NW}). The plots comparing the models to results have bands (Figure 5) reflecting these bounds.

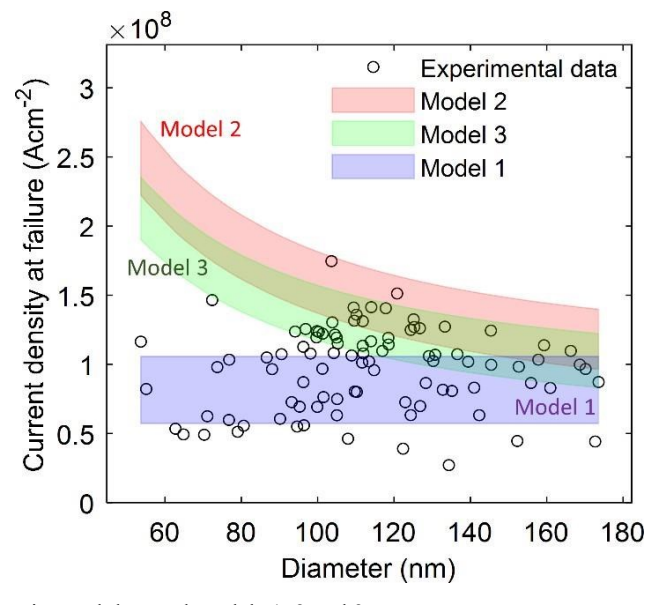


Figure 5: Comparison between the experimental data and models 1, 2 and 3.

The value of j_{fail} found in equation 7 represents an extreme case, when heat transfer to the substrate is not effective and only the contacts provide a heat sink. Note that it does not depend on nanowire diameter, given that the boundary condition applied at the

nanowire contacts scales with the diameter. Nanowires close to this model probably had non-optimal thermal contact to the substrate (see discussion). The predictions of this model (with the property bounds discussed above) are compared to the results in Figure 5.

3.2.2. Model 2: maximum heat transfer to the surrounding substrate and electrodes

We start again with the heat equation in cylindrical coordinates [31]:

$$\frac{\partial^2 \Delta T(r,z)}{\partial r^2} + \frac{1}{r} \frac{\partial \Delta T(r,z)}{\partial r} + \frac{\partial^2 \Delta T(r,z)}{\partial z^2} = -p\theta \left(r - \frac{d}{2}\right)$$

In the event where there is heat transfer to the substrate, the boundary condition will simply state that the heat flux in nanowire and the heat flux in substrate at the interface of the nanowire and the substrate is equal. Thus, we can write:

$$\kappa_{NW} \frac{\partial \Delta T(r,z)}{\partial r} \Big|_{r=\frac{d}{2}} = \kappa_s \frac{\partial \Delta T(r,z)}{\partial r} \Big|_{r=\frac{d}{2}}$$

$$9$$

The temperature, in this case, will remain a function of both r and z. Applying the boundary condition in 8, plus also assuming that the temperature of the surrounding medium is T_{room} at z = L/2, the solution to equation 8 at z = 0 and r = 0, representing the location where the temperature is maximum, can be expressed as [31]:

$$\Delta T(0,0) = \frac{4j^2 \rho M}{\kappa_{NW} L}$$
 10

Where,

$$M = \sum_{n=1,3,5,\dots}^{\infty} \sin\left(\frac{n\pi}{2}\right) \left(\frac{L}{n\pi}\right)^{3} \left[1 - \frac{\beta K_{1}(\frac{n\pi d}{2L})}{I_{1}(\frac{n\pi d}{2L})K_{0}(\frac{n\pi d}{2L}) + \beta I_{0}(\frac{n\pi d}{2L})K_{1}(\frac{n\pi d}{2L})}\right]$$
 11

This term, M, which includes modified Bessel functions of different orders (I_i, K_i) was calculated with MATLAB (see Supp. Mat.). $\beta = \kappa_s/\kappa_{NW}$. Let us express $\Delta T(0,0) = T_{melt} - T_{room}$. At this temperature, current density, $j = j_{fail}$. Finally, from equation 10:

$$j_{fail} = \sqrt{\frac{L}{4M}} \left[\frac{(T_{melt} - T_{room}) \kappa_{NW}}{\rho} \right]$$
 12

Due to the assumptions of maximum contact (and heat transfer) with the substrate, and electrodes considered to be held at T =

 T_{room} , this model gives the opposite extreme of Model 1 for the Joule heating of nanowires. In other words, this model provides the largest possible current density at failure. The red area represents model 2 in figure 4. We can establish from the red area that model 2 predicts an increase in current density at failure with a decrease in diameter. As we can see from equation 12, current density at failure, j_{fail} has an inverse relationship with M, which is a function of diameter d. As d decreases, surface area to volume ratio increases and hence, heat dissipation to generation ratio also increases. In other words, as the diameter decreases, nanowires are better able to transfer heat to the substrate. This heat transfer becomes prominent in the lower diameter region even with a relatively lower thermal conductivity of the substrate.

3.2.3. Model 3: partial substrate contact

Another model was proposed by Hunley et al. [32]. This model is closer to our experimental conditions as shown in the schematic of Figure 4c. Also, this model does not consider the electrical contacts to be held at $T = T_{room}$ but rather leaves it as an output of calculation. Modifications were made to account for our geometric configuration.

Model 3 can be described by equating the heat generated within an infinitesimal element $\frac{dQ_r}{dt}$, to the heat loss in the nanowire itself $\frac{dQ_n}{dt}$ and heat loss to the substrate $\frac{dQ_s}{dt}$, at steady state. Thus, we can write:

$$\frac{dQ_r}{dt} - \frac{dQ_s}{dt} - \frac{dQ_n}{dt} = 0$$

This equation can be expressed as:

$$\nabla^2 \Delta T(x) - m_1^2 \Delta T(x) + \frac{j^2 \rho}{\kappa_{NW}} = 0$$
14

where

$$m_1^2 = \frac{\pi \kappa_s}{A_{NW} \kappa_{NW} ln \left[\frac{D}{a} (2 + \pi) + e^{-\frac{2D}{a}} \right]}$$
 15

Where A_{NW} is the cross-sectional area of the nanowire. The solution of this equation is of the form:

$$\Delta T_{wire}(x) = 2C_1 cosh(m_1 x) + \frac{j^2 \rho}{\kappa_{NW} m_1^2}$$
 16

where, C_1 is a constant determined by applying appropriate boundary conditions. The boundary conditions and the methodology followed to determine C_1 are discussed in detail in the supplementary material. We can write the expression for C_1 as follows:

$$C_1 = \frac{j^2 \rho S}{\kappa_{NW} m_1^2} \tag{17}$$

Where,

$$S = -\frac{m_2(1 - \frac{2}{2+\pi})K_1(\frac{m \cdot 2d}{2+\pi})}{2m_1K_0(\frac{m \cdot 2d}{2+})\sinh(\frac{m \cdot 1L}{2}) + 2m_2(1 - \frac{2}{2+\pi})K_1(\frac{m \cdot 2d}{2+})\cosh(\frac{m \cdot 1L}{2})}$$
18

Here,
$$m_2 = \sqrt{\frac{\kappa_s}{\kappa_c \tau_c D}}$$
 19

Where, κ_c is the thermal conductivity of the electrical contacts. $\kappa_c = \kappa_{NW}$ since the electrical contacts are also fabricated with silver. $\tau_c = 105 \ nm$ is the thickness of electrical contacts and $D = 300 \ nm$ is the thickness of the substrate, which is assumed to be equal to the thickness of silicon dioxide insulation.

Now, substituting the value of C_1 into equation 16, we get:

$$\Delta T_{wire}(x) = (\frac{j^2 \rho}{\kappa_{NW} m_1^2}) \left[1 + 2S cosh(m_1 x) \right]$$
 20

The maximum temperature in the nanowire occurs at x = 0. At that location, we can substitute ΔT_{wire} by $(T_{melt} - T_{room})$ and j by j_{fail} . Thus, we can get an equation for j_{fail} :

$$j_{fail} = \sqrt{\frac{m_1^2}{(1+2S)}} \left[\frac{(T_{melt} - T_{room})\kappa_{NW}}{\rho} \right]$$
 21

The green area represents model 3 in figure 4. Here, as we have seen for model 2, we notice an increasing trend of current density at failure with a decrease in diameter as well. Thus, j_{fail} for model 3 has also an inverse relationship with diameter, which happens because contact area (with the substrate) to volume ratio increases with the decrease in diameter. In other words, the behaviour is fundamentally similar to Model 2, except the area available for heat transfer to the substrate is smaller.

3.3. Discussion: comparison of theoretical models with the experimental data

From Figure 5, we can see that most of the data is bound by the lower bound of model 1 and the upper bound of model 2, which confirms that these two models give extreme bounds for current density at failure. Since these models were representative of Joule heating, the results suggest this was the primary failure mode in our experiments.

Most of the experimental data lies within the blue region representing model 1. Model 1 represents perfect heat transfer to electrodes and zero heat transfer to the substrate. The true value for model 1 lies somewhere in between the blue area. Thus, a significant portion of the nanowires do not have optimal heat transfer to the substrate. The most likely reason is a thin polymer layer of a few nanometers (Polyvinyl pyrrolidone – PVP), which is present around the nanowires as a by-product of the synthesis [7]. This layer is critical in preserving the long-term stability of the nanowires (silver tarnishes in atmospheric air), but the results show that it impacts heat transfer, because if heat transfer to the substrate was optimal, more nanowires would fall within Model 3 area (green region). Besides, PVP has significantly lower thermal conductivity $(0.27 Wm^{-1}K^{-1})$ [35] compared to silicon dioxide (1.153 $Wm^{-1}K^{-1})$ [36].

The scatter of the data around model 1 can also be attributed to variable coverage of the PVP, introducing variations in heat transfer for different nanowires through the substrate. TEM images of the nanowires reveal that the PVP layer has small variations in thickness (Figure 7a). The variation can also happen at the interface of nanowires and the electrodes. The PVP was mostly removed in these areas since reliable electrical connections were achieved, which is shown by a steady contact resistance for all the data in Figure 6, except for the group of data representing the lowest current density at failure. The existence of this latter group of data, showing highest contact resistance for lowest current density at failure, indicates variations in PVP removal resulting in variable heat transfer to the electrodes. Since the nanowires that had the lowest PVP removal, and presumably worst contact between the nanowire and the metal electrode, would tend to achieve the highest contact resistance, it can be deduced from the plot that they would have the lowest current density at failure creating the scatter around model 1.

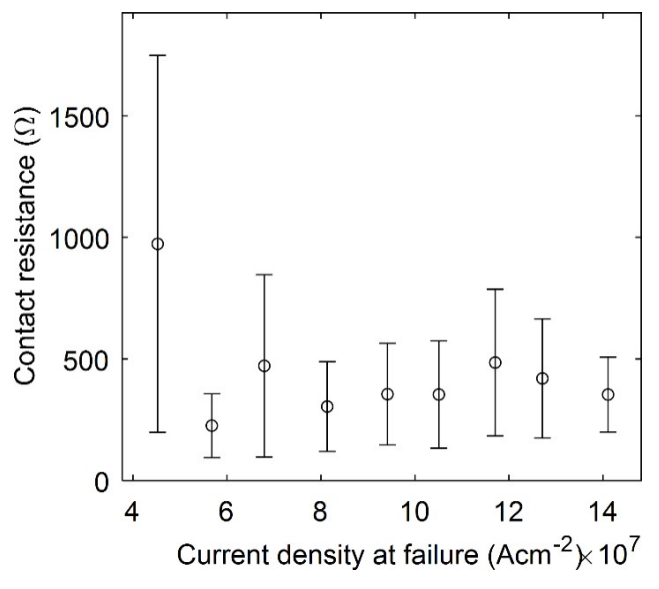


Figure 6: Average contact resistance vs. current density at failure. Data were grouped into current density bins.

Model 3 represents a more realistic condition with partial substrate contact. Nanowires lying in this area and between this area and Model 1 had better substrate contact. Some of the experimental data are in the green region representing model 3. However, the bulk of the data is below this region.

Local surface defects also explain why the nanowires experienced relatively lower current density at failure than what is predicted by model 3. It is well-established that twinned silver nanowires have minute surface undulations, which impact their mechanical properties as they lead to local stress concentrations [7,37]. We established, using TEM imaging, that the nanowires used in this study also display these surface defects as shown in Figure 7b. Just like for mechanical strength, undulations will impact current density at failure. A surface undulation locally reduces the cross-sectional area. As a result, although the same current is passing through the whole nanowire, the location with the defect experiences a higher local current density and hence a higher temperature compared to other locations. We observe increased scatter below 140 nm diameter, which is consistent with the fact that the cross-sectional area of smaller-diameter nanowires is proportionally reduced more, and thus is more sensitive to surface undulations.

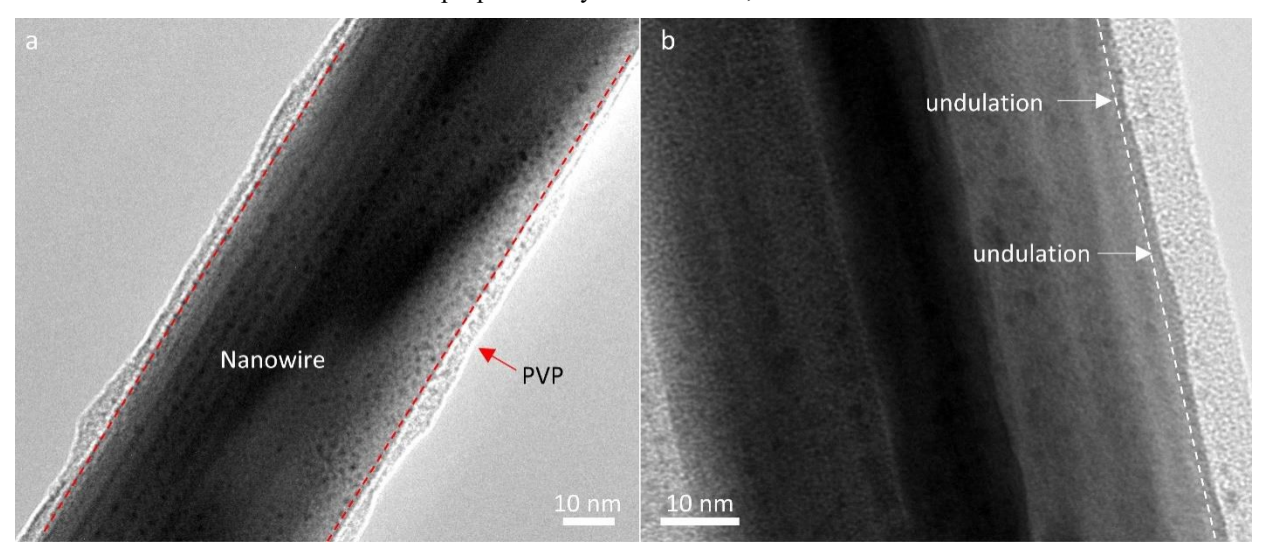


Figure 7: TEM images of silver nanowires showing a. the variation in PVP coverage. b. surface undulations. The dashed lines are guides to the eye to detect the variations.

All these reasons contribute to the observation that the bulk of the data points are lower than model 3. We summarize the reasons as local defects and less-than-optimal heat transfer due to PVP.

Model 2 is an upper bound on behavior, given that a medium surrounds the whole nanowire. As such, it is not surprising almost no nanowires surpass this bound. However, it is interesting that a few nanowires are within the envelope of model 2. We speculate these nanowires might have a confluence of favorable conditions; namely good substrate thermal contact, caused by a thin PVP layer; good electrode contact, and low or non-existent surface undulations. Furthermore, they might represent the intrinsic capabilities of twinned silver nanowires [38]. However, it is clear that extrinsic factors related to synthesis (PVP layer, surface undulations) need to be minimized for this potential intrinsic capability to be fully revealed. Note that these factors are common to several commercial and lab-synthesized nanowires [37] and not particular to the nanowires used in our study.

In general, the failure current densities were in the range of $(0.27 - 1.8) \times 10^8 \text{ Acm}^{-2}$. For context, current densities at failure for copper nanowires fabricated with e-beam lithography on a Si/SiN substrate were found to be in the range of $(1.3 - 1.6) \times 10^8 \text{Acm}^{-2}$ [16]. Electrodeposited bismuth nanowires failed in the range of $(0.5 - 3.5) \times 10^6 \text{ Acm}^{-2}$ [17]. Electrochemically deposited gold nanowires had failure current densities in the range of $(0.1 - 1.2) \times 10^8 \text{ Acm}^{-2}$ [14].

4. CONCLUSION

Our research shows that the current density at failure for penta-twinned silver nanowires has the potential to increase with a decrease in diameter, but is also affected by a high level of variability. The variability is brought upon by variations in the polymer coverage of the nanowires, a byproduct of the synthesis, and surface undulations. Surface undulations in particular, lead to larger variations for smaller diameters. Polymer coverage has an impact in heat transfer to the substrate, while undulations introduce local

variations in current density. An increase in reliability is thus intimately related to an improvement of heat transfer characteristics, potentially by removing the polymer coverage byproduct and replacing it by the encapsulating material in the flexible/stretchable electronic device.

These results provide guidelines for design of flexible/stretchable and transparent electronics devices. Lower current densities at failure, but more repeatability or consistency in behavior, would be obtained by using larger-diameter (>140 nm) nanowires in devices. Larger current densities at failure might be possible at lower diameters, but more stringent control of synthesis conditions is required for extrinsic factors such as PVP coverage (which impacts heat transfer), and surface undulations, to be minimized. In all cases, but especially for lower diameters, embedding the nanowires in a medium would be advantageous over exposed nanowires, as inefficient heat transfer will lead to localized failure of some nanowires, with a subsequent increase of current densities in other nanowires in the network, thus creating a positive feedback to failure [18,39].

ACKNOWLEDGEMENTS

This work was supported by the National Science Foundation (Award # 1807686). The authors would also like to thank the staff of UT Dallas Clean Room for instrument support.

REFERENCES

- [1] Sannicolo T, Lagrange M, Cabos A, Celle C, Simonato J-P and Bellet D 2016 Metallic Nanowire-Based Transparent Electrodes for Next Generation Flexible Devices: a Review *Small* **12** 6052–75
- [2] Venkataraman A, Amadi E V, Chen Y and Papadopoulos C 2019 Carbon Nanotube Assembly and Integration for Applications *Nanoscale Res. Lett.* **14** 220
- [3] Gudur A and Ji H-F 2016 Bio-Applications of Nanopillars Front. Nanosci. Nanotechnol. 2 1–10
- [4] Li B, Ye S, Stewart I E, Alvarez S and Wiley B J 2015 Synthesis and Purification of Silver Nanowires To Make Conducting Films with a Transmittance of 99% *Nano Lett.* **15** 6722–6
- [5] Ye S, Rathmell A R, Chen Z, Stewart I E and Wiley B J 2014 Metal Nanowire Networks: The Next Generation of Transparent Conductors *Adv. Mater.* **26** 6670–87
- [6] Zhu Y, Qin Q, Xu F, Fan F, Ding Y, Zhang T, Wiley B J and Wang Z L 2012 Size effects on elasticity, yielding, and fracture of silver nanowires: In situ experiments *Phys. Rev. B* **85** 045443
- [7] Filleter T, Ryu S, Kang K, Yin J, Bernal R A, Sohn K, Li S, Huang J, Cai W and Espinosa H D 2012 Nucleation-Controlled Distributed Plasticity in Penta-twinned Silver Nanowires *Small* 8 2986–93
- [8] Qin Q, Yin S, Cheng G, Li X, Chang T-H, Richter G, Zhu Y and Gao H 2015 Recoverable plasticity in penta-twinned metallic nanowires governed by dislocation nucleation and retraction *Nat. Commun.* **6** 5983
- [9] Bernal R A, Aghaei A, Lee S, Ryu S, Sohn K, Huang J, Cai W and Espinosa H 2015 Intrinsic Bauschinger Effect and Recoverable Plasticity in Pentatwinned Silver Nanowires Tested in Tension *Nano Lett.* **15** 139–46
- [10] Song L, Myers A C, Adams J J and Zhu Y 2014 Stretchable and Reversibly Deformable Radio Frequency Antennas Based on Silver Nanowires *ACS Appl. Mater. Interfaces* **6** 4248–53
- [11] Lagrange M, Sannicolo T, Muñoz-Rojas D, Lohan B G, Khan A, Anikin M, Jiménez C, Bruckert F, Bréchet Y and Bellet D 2017 Understanding the mechanisms leading to failure in metallic nanowire-based transparent heaters, and solution for stability enhancement *Nanotechnology* **28** 055709
- [12] Yagi M and Shirakashi J 2019 Quantifying Joule Heating and Mass Transport in Metal Nanowires During Controlled Electromigration *Materials (Basel)*. **12** 310
- [13] Tu K-N 2010 Electromigration in metals *Electronic Thin-Film Reliability* ed T Wong and G Dutfield (New York: Cambridge University Press) pp 237–69
- [14] Karim S, Maaz K, Ali G and Ensinger W 2009 Diameter dependent failure current density of gold nanowires *J. Phys. D. Appl. Phys.* **42** 185403
- [15] Aherne D, Satti A and Fitzmaurice D 2007 Diameter-dependent evolution of failure current density of highly conducting DNA-templated gold nanowires *Nanotechnology* **18** 125205
- [16] Huang Q, Lilley C M, Bode M and Divan R 2008 Surface and size effects on the electrical properties of Cu nanowires *J. Appl. Phys.* **104** 023709
- [17] Cornelius T W, Picht O, Müller S, Neumann R, Völklein F, Karim S and Duan J L 2008 Burnout current density of bismuth nanowires *J. Appl. Phys.* **103** 103713
- [18] Bellew AT, Manning HG, Gomes da Rocha C, Ferreira MS and Boland JJ 2015 Resistance of Single Ag Nanowire

- Junctions and Their Role in the Conductivity of Nanowire Networks ACS Nano 9 11422–9
 - [19] Sun Y, Yin Y, Mayers B T, Herricks T and Xia Y 2002 Uniform Silver Nanowires Synthesis by Reducing AgNO 3 with Ethylene Glycol in the Presence of Seeds and Poly(Vinyl Pyrrolidone) *Chem. Mater.* **14** 4736–45
 - [20] Yao S, Ren P, Song R, Liu Y, Huang Q, Dong J, O'Connor B T and Zhu Y 2020 Nanomaterial-Enabled Flexible and Stretchable Sensing Systems: Processing, Integration, and Applications *Adv. Mater.* **32** 1902343
 - [21] Myers A C, Huang H and Zhu Y 2015 Wearable silver nanowire dry electrodes for electrophysiological sensing *RSC Adv.* **5** 11627–32
 - [22] Koleśnik M M, Hansel S, Lutz T, Kinahan N, Boese M and Krstić V 2011 Resolving In Situ Specific-Contact, Current-Crowding, and Channel Resistivity in Nanowire Devices: A Case Study with Silver Nanowires *Small* 7 2873–7
 - [23] Johnson C J, Dujardin E, Davis S A, Murphy C J and Mann S 2002 Growth and form of gold nanorods prepared by seed-mediated, surfactant-directed synthesis *J. Mater. Chem.* **12** 1765–70
 - [24] Mei J, Haug R, Lanier O, Grözinger T and Zimmermann A 2018 Effect of Joule heating on the reliability of solder joints under power cycling conditions *Microelectron*. *Reliab*. **88–90** 684–90
 - [25] Schlitz R A, Yoon K, Fredin L A, Ha Y, Ratner M A, Marks T J and Lauhon L J 2010 Weibull Analysis of Dielectric Breakdown in a Self-Assembled Nanodielectric for Organic Transistors *J. Phys. Chem. Lett.* **1** 3292–7
 - [26] Tu K N, Liu Y and Li M 2017 Effect of Joule heating and current crowding on electromigration in mobile technology *Appl. Phys. Rev.* **4** 011101
 - [27] Bernal R A 2021 On the application of Weibull statistics for describing strength of micro and nanostructures *Mech. Mater.* **162** 104057
 - [28] Saleh M E, Beuth J L and de Boer M P 2014 Validated Prediction of the Strength Size Effect in Polycrystalline Silicon Using the Three-Parameter Weibull Function ed V Sglavo *J. Am. Ceram. Soc.* **97** 3982–90
 - [29] Callaway E B and Zok F W 2018 Weibull parameters obtained from dependence of fiber strength on fiber length and area *J. Am. Ceram. Soc.* **101** 4719–31
 - [30] Cook R F and DelRio F W 2019 Determination of ceramic flaw populations from component strengths *J. Am. Ceram. Soc.* **102** 4794–808
 - [31] Léonard F 2011 Reduced Joule heating in nanowires *Appl. Phys. Lett.* **98** 103101
 - [32] Hunley D P, Johnson S L, Flores R L, Sundararajan A and Strachan D R 2013 Analytical model for self-heating in nanowire geometries *J. Appl. Phys.* **113** 234306
 - [33] Ramasamy P, Seo D-M, Kim S-H and Kim J 2012 Effects of TiO2 shells on optical and thermal properties of silver nanowires *J. Mater. Chem.* **22** 11651
 - [34] Mayoral A, Allard L F, Ferrer D, Esparza R and Jose-Yacaman M 2011 On the behavior of Ag nanowires under high temperature: in situ characterization by aberration-corrected STEM *J. Mater. Chem.* **21** 893–8
 - [35] Xie X, Li D, Tsai T H, Liu J, Braun P V. and Cahill D G 2016 Thermal Conductivity, Heat Capacity, and Elastic Constants of Water-Soluble Polymers and Polymer Blends *Macromolecules* **49** 972–8
 - [36] Kato R and Hatta I 2005 Thermal conductivity measurement of thermally-oxidized SiO2 films on a silicon wafer using a thermo-reflectance technique *Int. J. Thermophys.* **26** 179–90
 - [37] Lee S and Ryu S 2015 Molecular Dynamics Study on the Distributed Plasticity of Penta-Twinned Silver Nanowires *Front.*Mater. 2 1–7
 - [38] Dong H, Xiao J, Melnik R and Wen B 2016 Weak phonon scattering effect of twin boundaries on thermal transmission *Sci. Rep.* **6** 19575
 - [39] Kholid F N, Huang H, Zhang Y and Fan H J 2016 Multiple electrical breakdowns and electrical annealing using high current approximating breakdown current of silver nanowire network *Nanotechnology* **27** 025703